Volume 12 | Number 38 | 14 October 2016 | Pages 7875–8060

Soft Matter

www.softmatter.org

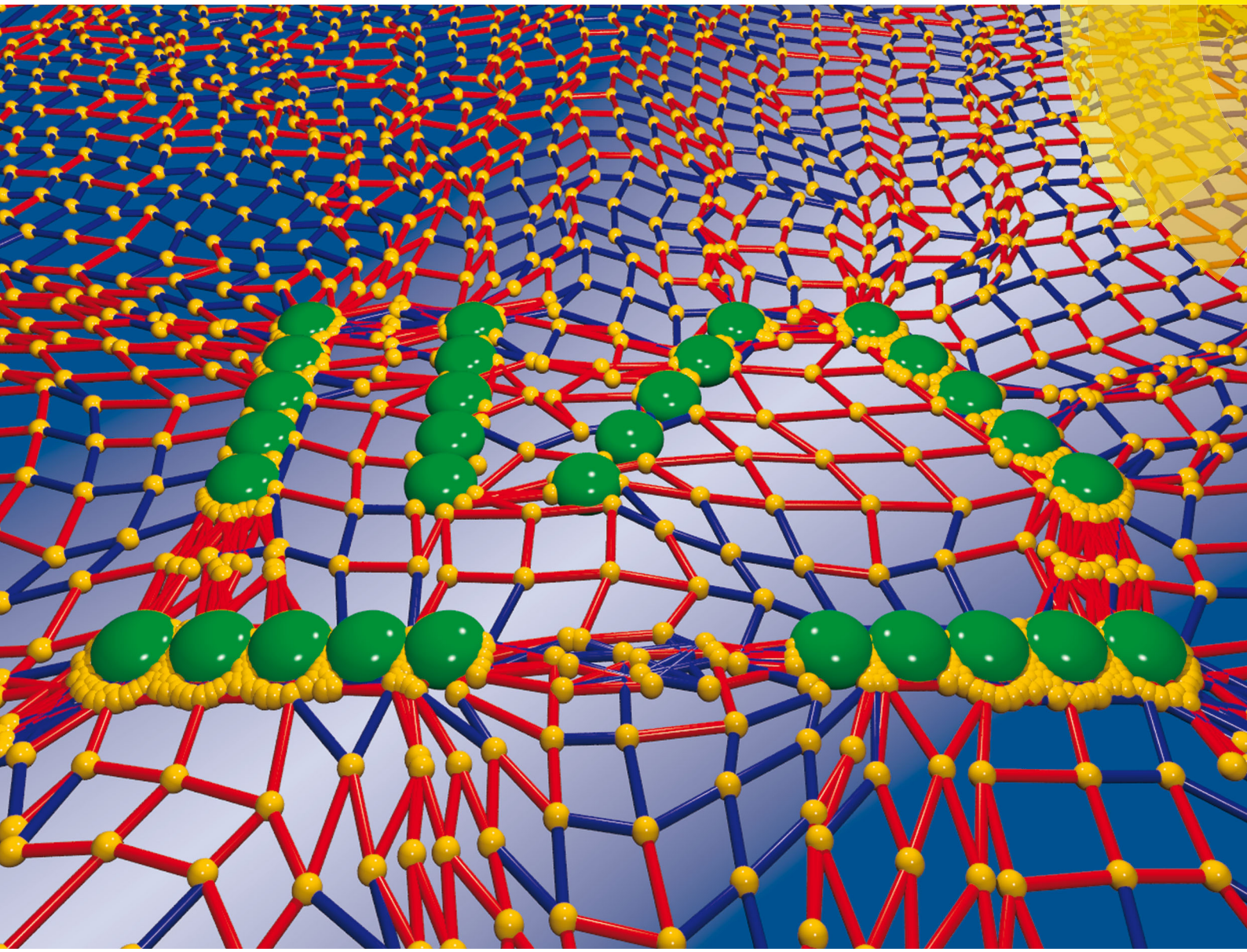

ISSN 1744-683X

ROYAL SOCIETY OF CHEMISTRY

PAPER
Ralf Metzler *et al.*
Interactions of rod-like particles on responsive elastic sheets

175 YEARS

Soft Matter

PAPER

View Article Online
View Journal | View Issue

CrossMark click for updates

Cite this: *Soft Matter*, 2016, 12, 7908

Interactions of rod-like particles on responsive elastic sheets

Surya K. Ghosh,[a] Andrey G. Cherstvy,[b] Eugene P. Petrov[c] and Ralf Metzler*[b]

Received 3rd July 2016,
Accepted 28th July 2016

DOI: 10.1039/c6sm01522k

www.rsc.org/softmatter

What are the physical laws of the mutual interactions of objects bound to cell membranes, such as various membrane proteins or elongated virus particles? To rationalise this, we here investigate by extensive computer simulations mutual interactions of rod-like particles adsorbed on the surface of responsive elastic two-dimensional sheets. Specifically, we quantify sheet deformations as a response to adhesion of such filamentous particles. We demonstrate that tip-to-tip contacts of rods are favoured for relatively soft sheets, while side-by-side contacts are preferred for stiffer elastic substrates. These attractive orientation-dependent substrate-mediated interactions between the rod-like particles on responsive sheets can drive their aggregation and self-assembly. The optimal orientation of the membrane-bound rods is established *via* responding to the elastic energy profiles created around the particles. We unveil the phase diagramme of attractive–repulsive rod–rod interactions in the plane of their separation and mutual orientation. Applications of our results to other systems featuring membrane-associated particles are also discussed.

Open Access Article. Published on 28 July 2016. Downloaded on 1/24/2026 1:41:57 AM.
This article is licensed under a Creative Commons Attribution 3.0 Unported Licence.

I. Introduction

What are the effects of membrane deformations and stresses arising upon binding of adhesive particles, what are the biological systems where such knowledge can be of importance, and how can we rationalise the effects of binding events using computer simulations? These are the key issues of the current paper.

Deformations and the mechanical response of elastic substrates such as cell membranes, synthetic membranes, or surfaces of hydrogels are recurrent themes in various area of biophysics, bioengineering, and biomedicine. Thus, novel diagnostic tools for the detection of pathogenic molecules—such as those based on surface binding of viruses and bacteria[1–5]—are highly desired for biochemical and biomedical purposes. Visual detection of the binding of pathogens often necessitates some responsive underlying substrates, such as those of membrane-like supports or hydrogels.[6] Some modern biosensors utilise lipid membranes to monitor binding of proteins.[7]

Membrane-facilitated supramolecular aggregation of, for instance, proteins and nanoparticles,[8–13] larger particles such as proteins and virus-like colloidal particles[14,15] as well as membrane-driven condensation of linear DNA on freestanding lipid bilayer[16–18] is ubiquitous in biophysics. Assembly and pattern formation of colloidal particles of various shapes and surface properties on liquid interfaces is also an active field of research.[19–23] With respect to the dynamical aspects of particle behavior on membranes, the non-Brownian diffusion of membrane lipids and membrane-associated proteins was also studied recently.[11,12,24–31]

The visual analogy between curvature-mediated interactions of particles on membranes and capillary-immersion interactions[19,32–34] is quite straightforward. The deformations of the surrounding of a particle immersed in a liquid scales with the liquid contact angle due to wetting. This is reminiscent of deformations of cationic lipid membranes triggered by, for instance, electrostatic binding[16–18,35–37] of oppositely charged DNA molecules and *fd* filamentous virus particles.[38] [Ref. 39 and 40 address DNA–lipid interactions not involving membrane deformations. Linear and knotted DNAs in confined two-dimensional environments were studied in ref. 41–45, see also ref. 46. DNA adsorption onto likely charged lipid surfaces mediated by divalent cations can also take place.[47]] The propensity of membrane wrapping around the particles scales with their mutual attraction strength, see ref. 18 and 48–60 for a theoretical viewpoint. Meniscus-shaped deformations for capillary interactions[13,19,20,61–65] are similar to out-of-plane bending deformations of lipid membranes which often trigger the aggregation of adsorbed particles.

Recently, we probed *via* computer simulations the interactions of adhesive disc-like particles with a two-dimensional elastic network by Langevin dynamics simulations.[66] We demonstrated

[a] *TIMC-IMAG Laboratory, Universite Grenoble Alpes, CNRS UMR, 5525 Grenoble, France*
[b] *Institute for Physics & Astronomy, University of Potsdam, 14476 Potsdam-Golm, Germany. E-mail: rmetzler@uni-potsdam.de*
[c] *Max-Planck Institute of Biochemistry, Department Cellular and Molecular Biophysics, 82152 Martinsried, Germany*

This journal is © The Royal Society of Chemistry 2016

Open Access Article. Published on 28 July 2016. Downloaded on 1/24/2026 1:41:57 AM.
This article is licensed under a Creative Commons Attribution 3.0 Unported Licence.

how far the network deformations propagate from an isolated particle upon its adhesion to the substrate and how the overlap of these deformations gives rise to inter-particle substrate-mediated interactions. The model parameters such as particle–network attraction strength and network elastic constant were varied in a wide range.[66]

We here extend this analysis to rod-like particles bound to elastic substrates and interacting *via* substrate deformations. This system mimics the orientation-dependent forces between negatively charged rod-like *fd* viruses adsorbed on freestanding cationic lipid membranes, as monitored recently by fluorescence video microscopy.[38] It was observed that *fd* viruses adsorbed onto a cationic lipid bilayer tend to form tip-to-tip linear aggregates.[38] At higher densities of adsorbed virus particles, also branched arrangements of viruses were observed.[38] Also, interesting findings of computer simulations appeared recently regarding the assembly of curved cylindrical particles on a model lipid vesicle *via* side-to-side *versus* tip-to-tip contacts,[67] also motivating the current research. Such *in vitro* virus–vesicle systems might shed light onto the properties of interactions of elongated viruses—including dangerous Ebola and Marburg viruses[68,69]—with the membranes of living cells.

One physical reason for the aggregation of rods is that the adsorbed particles tend to minimise the elastic energy—accumulated particularly around their tips—*via* connecting the ends. This reduces the highly curved area of the underlying membrane. Another reason—that might be relevant particularly in very low salt solutions used in experiments[38]—are the repulsive electrostatic interactions[70–73] between the highly charged *fd* viruses. The latter are evidently stronger for the very close side-by-side contacts as compared to tip-to-tip contacts, at least for uniformly charged rods.[74] The reader is also referred to ref. 75–77 for interactions of skewed charged helices and to ref. 78–81 for electrostatics of lipid membranes. We neglect here electrostatic effects, focusing on substrate-mediated forces. We show that already in this case either tip-to-tip or side-by-side conformations are favourable, depending on the model parameters. Our results are important for the understanding of the complete scenario, with both membrane elasticity and inter-particle electrostatics being included.

Another motivation comes from recent results of linear *versus* side-by-side assembly of BAR (Bin/Amphiphysin/Rvs) proteins on elastic membranes.[9,10] The coarse-grained molecular dynamics simulations showed[10] that strong protein–membrane adhesion favours tip-to-tip protein assembly, while larger membrane tensions rather facilitate the formation of aggregates with side-by-side contacts. Larger membrane tensions were shown to maximise the contact surface of aggregating proteins. In simulations on tensionless membranes, the proteins mostly form tip-to-tip aggregates.[123]

One more motivation for biomembranes with nonzero tension comes from pulmonary surfactants[82–84] which help to control the surface tension of alveolar cells in lungs. The membrane is then under a continuously varying time dependent tension, due to the respiratory cycle. Note that pulmonary surfactant layers can host potentially pathogenic rod-like particles of asbestos fibers, nanotube fibers, *etc.*, making the current investigation relevant in this context as well.

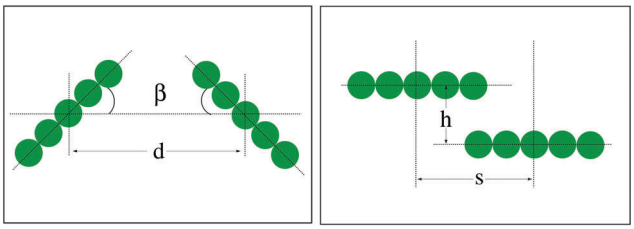

Fig. 1 Rotation and sliding scheme of membrane-adhered rods (view from the top). Here, for rotating rods β designates the mutual orientation angle and d is the particle–particle distance with respect to their centre of mass. For sliding rods, h is the inter-axial separation between the particles (offset distance) and s is the sliding distance.

The curvature-driven orientation, migration, and steering of asymmetric particles (rods in particular) in external gradient fields was also examined experimentally and exploited theoretically in terms of capillary forces in ref. 33. The particles were shown to migrate along the interface to minimise the elastic energy *via* sensing the principal radii of curvature of the surface deformations. Also, the formation of linear aggregates of nanoparticles adsorbed on fluid membranes is often energetically beneficial over the disc-like agglomeration.[20,21] The interface distortions created by adsorbed rod-like particles were shown to be capable of aligning the particles along the principle axis of curvature. Inter-particle interactions cause a pronounced tip-to-tip assembly of the rods *via* reducing the penalty of high-curvature regions.[20] With respect to string formation by capillary interactions, the reader is referred to ref. 32, 34 and 65.

Gravity-mediated interactions caused by interface deformations were shown to be pronounced for up to micron-size particles of spherical and elongated shapes. In particular, capillary quadrupolar forces are capable of forming chains of aggregated rods.[22] Regarding the variation of inter-particle interactions with the distance, the interaction energies of up to $\sim 10^5\ k_BT$ with the dependence $E_{int}(r) \sim r^{-4}$ on the inter-particle separation r were predicted experimentally for tip-to-tip interactions of ~ 10 μm long and ~ 1 μm thick ellipsoidal particles.[22] This power-law scaling is consistent with quadrupolar interface-mediated interactions between spherical particles.[23,85–87]

The current paper is organised as follows. In Section II we present the detailed description of the simulation procedure. In Section III we describe the main results of the computer simulations concerning the substrate deformations and the resulting rod–rod interaction energies. The latter are evaluated for systematically varying mutual orientation of the particles β, network elasticity constant k, rod–rod separation d and the sliding distance h when the adsorbed rods pass one another (see Fig. 1). Our principal result is the phase diagramme in the plane $\{\beta, d\}$. In Section IV we discuss the implications of our results to some biophysical systems, in particular to the assembly of rod-like colloidal particles on lipid membranes.

II. Model and approximations

Using the same procedure as in our study of interactions of small disc-like particles on responsive two-dimensional elastic

Open Access Article. Published on 28 July 2016. Downloaded on 1/24/2026 1:41:57 AM.
This article is licensed under a Creative Commons Attribution 3.0 Unported Licence.

sheets,[66] we here simulate the surface-mediated forces between rod-like particles, as shown in Fig. 1. Namely, we use a discrete two-dimensional lattice-based model to study the deformations in elastic networks by the Langevin dynamics simulations. Every network bead has a unit radius σ. The network consists of a square lattice of spherical beads inter-connected by elastic springs. The lattice of size n contains $(n+1)^2$ beads and $2n(n+1)$ elastic bonds. The system size in simulations is $n = 25$, to minimise finite size effects. If considering rods at even larger centre-to-centre distances d, larger elastic sheets can be necessary. Each bead of the network is subject to thermal fluctuations. In our model, the network deformations triggered by particle binding occur only in the $\{x, y\}$ plane.

Let us shortly discuss the relevance of our two-dimensional elastic sheets to membrane-based physical systems. In reality, upon particle–membrane binding progressive out-of-plane deformations and wrapping of membranes[13,15,18,57,58,88–90] around adhering particles often takes place. To account for them, a three-dimensional membrane model is required. Our model of in-plane deformations can be considered as a "projection" of the Monge representation[80,91] for the membrane height deformations $\tilde{h}(x, y)$ acting against the surface tension Σ, where the membrane deformation energy is $E_{\mathrm{el}}(\tilde{h}) \sim (\Sigma/2)\int \mathrm{d}x\mathrm{d}y\left[\left(\partial\tilde{h}/\partial x\right)^2+\left(\partial\tilde{h}/\partial y\right)^2\right]$. A physically more adequate model—with all modes of membrane deformations accounted for, with periodic boundary conditions for the elastic sheets and for realistic length-to-thickness ratio of rod-like particles – is the goal for our future studies.[92,124]

Our substrate contains elastically stretchable links that ensure the network response to the particle binding. Realistic lipid membranes are, in contrast, barely stretchable and their elastic deformations in response to particle binding is mainly out-of-plane bending. Yet, the area of cell membranes can change by some 5 to 10%.[93] The application of strain to surface-adhered cells "flattens" membrane undulations, leading for some cell types to up to 10% surface area change.[94] The adaptation of cell membranes to stretching and osmotic shocks involves volume and area changes, required *e.g.* for cell spreading and membrane protrusions.[95–97] The resilience of cell membranes to pressure differences is much better for bacterial and plant cells, as compared to animal cells.[95] Also note that the actomyosin cortex beneath the membrane actively controls the cell volume and—importantly—the degree of membrane fluctuations. For membrane vesicles, for instance, these surface undulations can be flattened by positive external tensions, applied *e.g. via* a micropipette aspiration.[98] Some applications of our results to stretchable synthetic membranes used *i.e.* for skin engineering and biosensor applications are also feasible.[99,100]

In our model system, the entire network is anchored at eight points, thus forming a pre-stretched sheet. We checked that increasing the number of anchoring points of the sheet to sixteen—representing a more homogeneous membrane boundary or larger elastic sheets—does not charge the trends for the rod–rod membrane-mediated interactions we present below. The elastic sheets used are large enough compared to the rod length, such that the elastic deformations are localised in the central region of the sheet, see Fig. 5. This setup maintains the shape of the elastic sheet and prevents its collapse onto attractive particles deposited, particularly for strong binding energies ε_{A}, see Fig. 2. For quite strong deformations this mimics an inherent tension in the network which is typically low but non-zero as encountered, for instance, for large membrane vesicles acting as simple cell models. Our system has some similarities to experimental systems of an elastic sheet supported by nanopillars[101,102] keeping it in a two dimensional configuration, lipid membranes adhered to micro-patterned substrates,[103] as well as pore-spanning lipid bilayers.[104] The reader is also referred here to the study[105] on the formation of membrane adhesion domains under external tension.

The rod-like particles in the simulations are linear arrays composed of spheres of diameter $2R = a = 4\sigma$, and are of total length of $l = 5a$ (measured in terms of the lattice constant a). The overall generic binding energy E_{A} of rod-like particles to the network beads mimics the interactions of responsive oppositely charged lipid membranes with filamentous viruses.[38] For wild-type *fd* viruses the particle diameter is $\approx$6.6 nm, the length is $\approx$880 nm, the persistence length is $\sim$2 μm,[106,107] and the length-to-thickness ratio is $\sim$130.[108–110] Some typical elastic energy distributions in the network are shown in Fig. 2 and 3.

The strength of adhesion of beads composing the rod-like particles to a bead on the network, ε_{A}, is parameterised by the

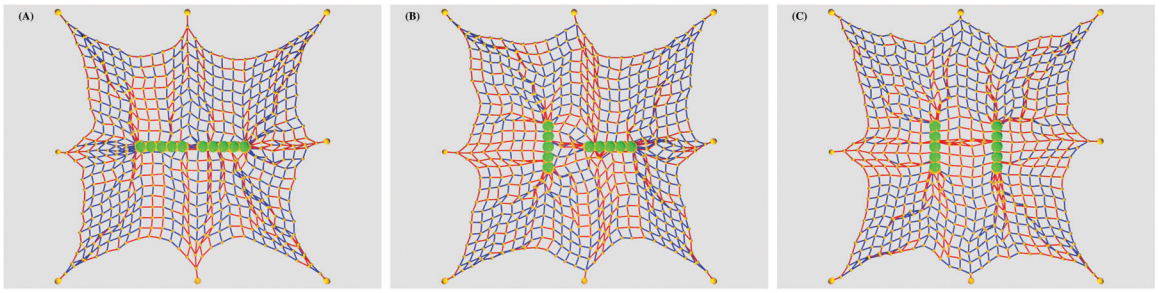

Fig. 2 Schematic of adhesive rods deposited on a responsive elastic sheet, anchored at eight points (snapshot). From left to right: the rods are oriented tip-to-tip, the rods are in perpendicular arrangement, and in parallel side-by-side configuration. The red and blue colours of the network springs signify stretched and compressed links of the network, respectively. The size of the network is $n = 25$, the elastic constant is $k = 45$, the rod length is $l = 5a$, and the rod–bead interaction strength is $\varepsilon_{\mathrm{A}} = 5$, see text for details.

 This journal is © The Royal Society of Chemistry 2016

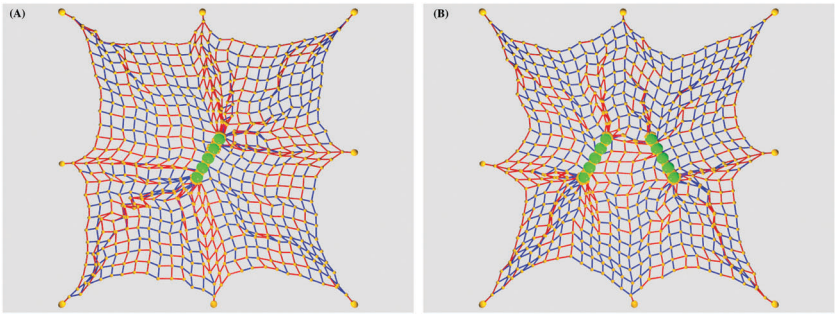

Fig. 3 Network deformation pattern in the vicinity of a single rod and two rods with simultaneously varied mutual angle $\beta_1 = \beta_2 = \beta$, evaluated at a single time moment for the parameters of Fig. 2.

Open Access Article. Published on 28 July 2016. Downloaded on 1/24/2026 1:41:57 AM.
This article is licensed under a Creative Commons Attribution 3.0 Unported Licence.

truncated 6–12 Lennard-Jones (LJ) potential. Namely, to model attractive inter-particle interactions we use

$$E_{\mathrm{attr}}(r) = 4\varepsilon_{\mathrm{A}}[(\sigma/r)^{12} - (\sigma/r)^{6}] + C_{\mathrm{A}}(\varepsilon_{\mathrm{A}}),$$

for $r < r_{\mathrm{cut}} = 2.5\sigma$ and $E_{\mathrm{attr}}(r) = 0$ otherwise. The constant C_{A} is adjusted such that the potential vanishes beyond the cutoff distance at $r > r_{\mathrm{cut}}$, see ref. 66 for details. The interactions between the network beads are represented by the standard Weeks–Chandler–Andersen repulsive LJ-like potential $E_{\mathrm{LJ}}(r)$.[111] A varying rod–sheet adhesiveness in the simulations mimics a tunable virus–membrane attraction in experiments,[38] achievable, *e.g.*, *via* a functionalisation of the virus surface proteins.

The dynamics of a bead $\{i,j\}$ of a two-dimensional network is governed by the Langevin equation

$$m\frac{\mathrm{d}^2\mathbf{r}_{ij}(t)}{\mathrm{d}t^2} = -\sum_{K}\nabla E_{\mathrm{attr}}\left(\left|\mathbf{r}_{ij} - \mathbf{R}_{\mathrm{v},K}\right| - \sigma/2 - R/2\right) - \sum_{p\neq i,q\neq j}^{(n+1)}\nabla\left[E_{\mathrm{LJ}}\left(\left|\mathbf{r}_{ij} - \mathbf{r}_{pq}\right| - \sigma\right)\right] - \xi\mathbf{v}_{ij}(t) + \mathbf{F}(t). \quad (1)$$

Here m is the bead mass, ξ is the friction coefficient, $\mathbf{v}_{ij}$ is the bead velocity, σ is the bead diameter, $\mathbf{R}_{\mathrm{v},K}$ is the position of the adhering Kth sphere of the rod. Also, every bead is subject to white Gaussian δ-correlated noise $\mathbf{F}(t)$ with $\langle\mathbf{F}(t)\cdot\mathbf{F}(t')\rangle = 4\xi k_{\mathrm{B}}T\delta(t - t')$ and zero mean. The rods are fixed at a given position and orientation on the network, while the dynamics of network beads is studied. Our simulations are performed with the velocity Verlet algorithm,[112] with the integration step $\Delta t = 0.001$. The time is counted in units of the standard elementary time.[112] We perform the averaging over time for each run and over $M \sim 500$ realisations for a given set of parameters.

The elastic deformation energy of bonds between neighbouring beads is parameterised by the harmonic spring potential, with the elasticity constant k assuming the values $k = 5$, 15, and 45. The elastic constants are in units of the thermal energy per lattice constant squared $k_{\mathrm{B}}T/a^2$, the energies and adhesion strengths ε_{A} are in units of $k_{\mathrm{B}}T$, and the distances are in units of the lattice constant a. The values of the model parameters corresponding to the sheet elasticity k and rod–sheet adhesion strength ε_{A} can be adjusted to be relevant to a given physical system, *e.g.* DNA[16] or *fd* viruses[38] adsorbed on lipid membranes.

By performing extensive Langevin Dynamics simulations we examine the surface-mediated interactions between strongly anisotropic rod-like particles adsorbed on a responsive substrate. We obtain the attraction–repulsion phase diagramme in the space of model parameters such as the rod–sheet adhesiveness, the sheet elasticity, and the rod–rod centre-to-centre separation. We unravel the dependence of the interaction energy on the mutual orientation angle β of the rods, $E_{\mathrm{int}}(\beta)$, see Fig. 1.

This energy is defined as the difference of the rod–sheet adsorption and network deformation energy of two interacting rods at the centre-to-centre distance d, with respect to the energies of individual rods adsorbed at the same positions on the sheet (self-energy). Thus, the interaction energy of the two particles at very large distances should vanish. It is however non-zero in our setups with a finite network size. Mathematically, in what follows we thus compute the energy difference

$$E_{\mathrm{int}}(\beta, d) = [E_{21,\mathrm{A}}(\beta, d) + E_{21,\mathrm{el}}(\beta, d)] - (E_{1,\mathrm{A}} + E_{1,\mathrm{el}}) - (E_{2,\mathrm{A}} + E_{2,\mathrm{el}}). \quad (3)$$

III. Main results

To calibrate our model system, we start by discussing the network deformations around a single rod adsorbed on the network. After this we consider two adsorbed rods at varying centre-to-centre separation d and orientation angle β. Finally, we study the rod–rod interaction energy as a function of the offset h and horizontal shift s. We consider below immobile rod-like particles deposited onto elastic sheets. The possible "modes" of particle motion we examine below control the interaction energy for the situations when the rods are allowed to diffuse on the substrate, as observed in experiments.[38] The results for the pair rod–rod membrane-mediated interaction potentials presented below can be applied and extended to study the behaviour of multiple membrane-adsorbed rod-like particles.

We observe that the extent of the sheet deformations induced upon rod binding is a sensitive function of the model parameters. Namely, for weak rod–substrate attraction the radius

Open Access Article. Published on 28 July 2016. Downloaded on 1/24/2026 1:41:57 AM.
This article is licensed under a Creative Commons Attribution 3.0 Unported Licence.

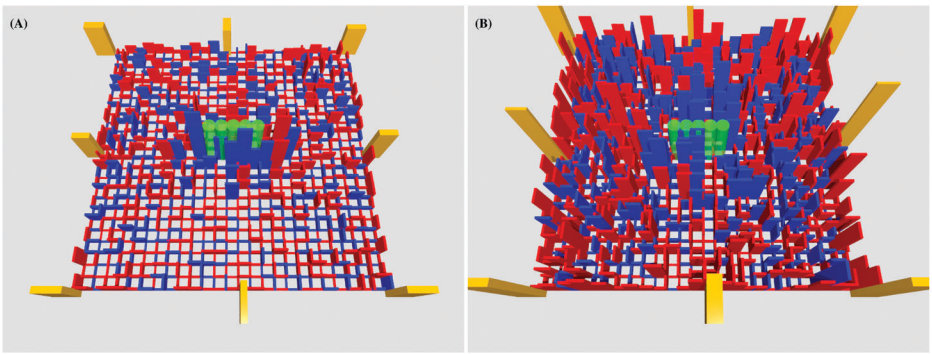

Fig. 4 Averaged network energy distribution around a substrate-adhered rod, evaluated for k = 45, ε_A = 5 (left panel, weak rod–sheet interactions) and k = 45, ε_A = 15 (right panel, strong rod–sheet interactions). The colour coding scheme is the same as in Fig. 2: the red and blue bars are stretching and compression energies in each link, the bar height is the energy magnitude. The energy in the anchor points is shown as yellow bars. The adsorbed rod is visible in the middle of each panel. The energy accumulated in all the anchors is about 60 and 132 k_BT for the left and right panel, respectively, so the energy of the inner-lattice deformations can be calibrated to these values. Other parameters: l = 5a and n = 25.

of propagation of the network deformations is relatively small and extensive deformations are localised near the rods, Fig. 4, see also ref. 125.

Conversely, for strong rod–sheet adhesion the network deformations are appreciable and the entire elastic sheet acquires extensive deformations. These are visualised in Fig. 4, in which the height of each bar represents the elastic energy accumulated in a given elastic link of the network. Particularly for strong rod–substrate attractions we find that the links between network beads are mainly compressed near the rod-like particle, while they are mainly stretched further away from the adsorbed rod, Fig. 4.

To quantify the propagation of the network deformations, we count the fraction of the elastic energy accumulated within the physical distance r from the rod centre, Fig. 5. We observe that—in response to binding of rods onto soft elastic sheets under conditions of strong rod–sheet binding—the elastic deformations are concentrated within a close proximity of the adsorbed rods. Thus, the total elastic energy grows faster with the separation r in this case. For stiffer networks the effect of ε_A on the decay length of deformations from the adsorbed rod becomes weaker, Fig. 5B.

In Fig. 6 we present the dependence of the rod–network adsorption energy on the mutual angle β of rotation of the two rods, see Fig. 1. We observe that for weak attractions (the squares in Fig. 6) the effect of binding is very local and the effect of angle variation is almost negligible. For large binding

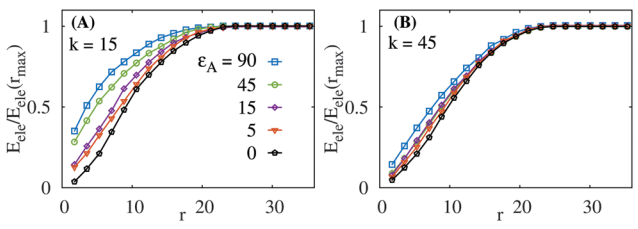

Fig. 5 Total elastic energy of the lattice deformations *versus* the physical distance r from the centre of a single rod for a range of adhesion strength ε_A. The results are normalised to the overall network energy. Elastic constants and attraction energies are indicated.

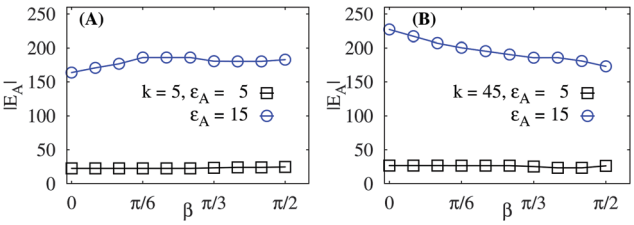

Fig. 6 Total rod–network adsorption energy E_A *versus* the rod–rod mutual orientation angle β, plotted for different sheet stiffness k and rod–network attraction ε_A. The left panel represents softer sheets. Larger rod–substrate attractions on stiffer sheets yield a stronger $E_A(\beta)$-dependence (right panel). Parameters are the same as in Fig. 5.

strengths the network deformations propagate over longer distances and we observe stronger effects due to variation of β. For stiff sheets (at k = 45, panel B of Fig. 6), at β = 0 only the regions close to the rod tips share the deformed network elements. At β = π/2, in contrast, the whole sheet region in between the two parallel rods is shared and deformed in the course of rod binding, hence we have a lower binding energy at larger angles β for stiff sheets. Note that for soft sheets the movement of the beads are much easier and thus the orientation effects of rods are less prominent.

To compute the mutual interaction energy $E_{int}(\beta, d)$ we vary both angles β of the rods, see Fig. 7. We observe that for relatively soft networks and weak rod–sheet adhesion strengths ε_A the tip-to-tip rod contacts (β = 0) yield stronger attractive energies as compared to side-by-side contacts (β = π/2), Fig. 7A. The energetic benefit of tip-to-tip arrangement is however rather moderate. We recall here that this mutual orientation was preferentially observed when *fd* viruses assemble on free-standing lipid membranes.[38] For stiff networks this trend disappears and E_{int} has a minimum for the parallel side-by-side arrangement, Fig. 7B. This is in line with the conclusion for preferred side-by-side contacts of rod-like proteins on rather stiff membrane-like elastic sheets.[10]

For stronger rod–sheet attraction (larger ε_A) the magnitude of the interaction energy increases. For soft sheets the network

 This journal is © The Royal Society of Chemistry 2016

Open Access Article. Published on 28 July 2016. Downloaded on 1/24/2026 1:41:57 AM.
This article is licensed under a Creative Commons Attribution 3.0 Unported Licence.

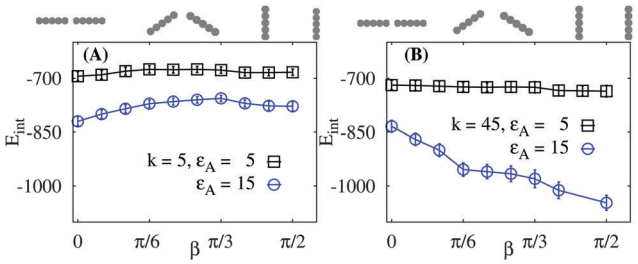

Fig. 7 Magnitude of the rod–rod network-mediated interaction energy *versus* orientation angle β. The respective rod conformations are depicted on the top of each panel. The magnitude of E_{int} grows with the rod–network attraction. For softer sheets and stronger attractions the tip-to-tip conformation is favourable, while for rigid elastic networks and large ε_A the side-by-side contacts are preferred. Other parameters are the same as in Fig. 5 and $d = 6a$. Within error bars, no maxima exists in panel A for intermediate β values.

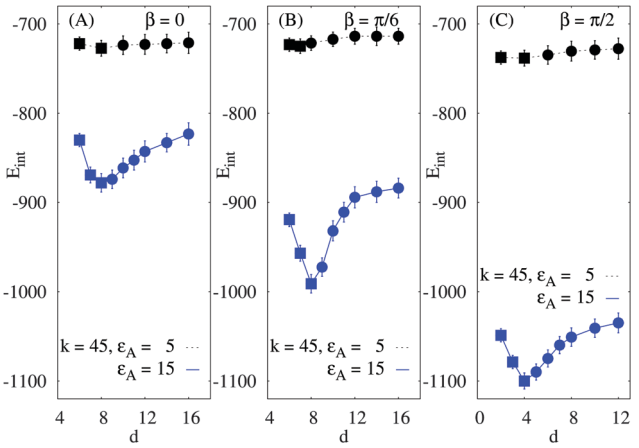

Fig. 8 Interaction energy $E_{int}(d)$ of substrate-adhered rods *versus* inter-axial distance d, plotted for $\beta = 0$, $\pi/6$, and $\pi/2$ (from left to right). Other parameters are indicated in the plots. The circles and squares designate the regions of attraction and repulsion, respectively. The error bars are shown.

deformations do not propagate far from the adsorbed rod, with the typical length scale of Λ, see ref. 123. Thus, for a fixed rod–rod distance $d = 6a$ as in Fig. 7 the overlap of the network deformations is only substantial when the tips of both rods are close. At these conditions and at a fixed d the side-by-side contacts result in weaker overlap of network deformations and thus in smaller magnitudes of the rod–rod interaction energy, E_{int}. Note that for larger d the dependencies $E_{int}(\beta)$ are similar to those in Fig. 7, but the energy magnitudes and its variations with β become smaller and less pronounced (not shown).

Thus, one expects that for several rods deposited and allowed to diffuse on soft networks the formation of linear tip-to-tip aggregates or branched structures will be favoured, as indeed observed for *fd* filamentous viruses on freestanding lipid membranes[38] and for elongated colloidal particles on air–liquid interfaces.[34] In contrast, for stiffer sheets—when the network deformations are of a longer range—rather side-by-side contacts of rods are beneficial. Aggregate formation by side-by-side contacts will form "caterpillar-like" structures of rods, as those observed due to capillary forces on air–liquid interfaces.[19]

Now, we consider the inter-rod interaction energy as a function of inter-rod separation, $E_{int}(d)$, for varying angle β of mutual orientation of the rods, see Fig. 8. We find that—particularly for stronger rod–sheet attractions—at intermediate-to-large rod–rod distances the substrate-mediated force between the fragments is attractive, that is $\partial E_{int}(d)/\partial d > 0$. At very close rod–rod distances this derivative is negative indicating repulsive forces, see also endnote.[126] The crossover distance between the region of long-ranged attraction and short-ranged repulsion corresponds to the distance of the energy minimum of elastically-mediated rod–rod interactions. Similar to substrate-mediated interactions of disc-like particles on similar elastic supports (see Fig. 10 in ref. 66), the rod–rod network-mediated interactions become stronger for stiffer sheets and larger rod–network adhesiveness, ε_A.

The behavior of the crossover region between the attractive and repulsive regimes as a function of the model parameters is presented in the state diagramme of Fig. 9. Here, we combine the $E_{int}(d)$ curves as in Fig. 8 and vary simultaneously the angle β and centre-to-centre distance centres d. We illustrate the parameter space where the network-adsorbed rods repel and attract one another. Both for soft and stiff elastic sheets—depicted respectively in Fig. 9A and B—we find the minimum in the rod–rod interaction energy $E_{int}(d)$.

For stiff elastic sheets the $\beta = \pi/2$ orientation and side-by-side arrangement of the rods is more energetically favourable, consistent with the energy–distance curves of Fig. 8. The energy minima are realised at somewhat larger inter-rod distances d, as compared to soft sheets, see the dashed line in Fig. 9. The interaction energy attains its minimum also at larger d as the orientation angle β decreases, see Fig. 9B where the dashed line separates the regions of rod–rod repulsion and attraction. Note that for small β values and short d separations the rods sterically overlap and such regions of the phase diagramme were not examined in Fig. 9.

For soft elastic sheets for all mutual rod–rod orientations we observe a clear minimum of the interaction energy over the rod–rod distance d. However, no clear preference of the energy well depth on the angular orientation of particles exists. In addition, the entire $E_{int}(d, \beta)$ variation is substantially smaller than for stiff sheets, see Fig. 9A. Therefore, for soft sheets the particles will tend to form flexible tip-to-tip aggregates on responsive substrates, similar to the structures observed experimentally.[38]

Note that it would be interesting to study the full dependence $E_{int}(d, \beta_1, \beta_2)$ for arbitrary uncorrelated orientation of rods on the elastic network. Note that for the capillary interactions of ellipsoidal particles along the elastic support both side-by-side and tip-to-tip interactions are attractive, while end-to-side contacts are repulsive. Physically, this attractive *versus* repulsive behaviour emerges due, correspondingly, to alike and opposite directions of the interface height deformations around the interface-adhered particles.[90]

Finally, we address the case of the two rods passing one another on the elastic sheet in a sliding fashion, at a fixed

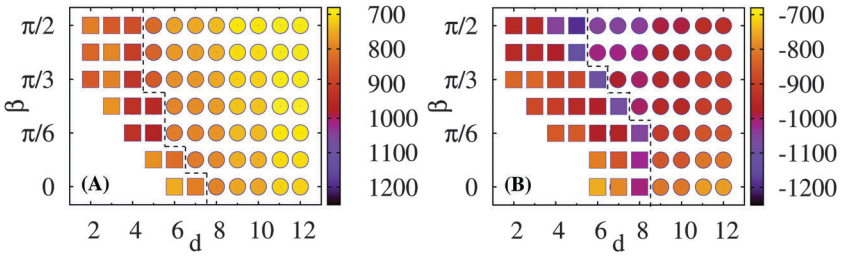

Fig. 9 Phase diagramme of network-bound rods plotted in the plane $\{\beta, d\}$. The squares (circles) represent the domain of rod–rod repulsion (attraction). The dashed curve is the position of $E_{int}(d)$ minimum, with the magnitude coded in the colour legend. The left and right panels correspond to soft and rigid elastic sheets, with $k = 5$ and $k = 45$ respectively, and $\varepsilon_A = 15$ in both panels.

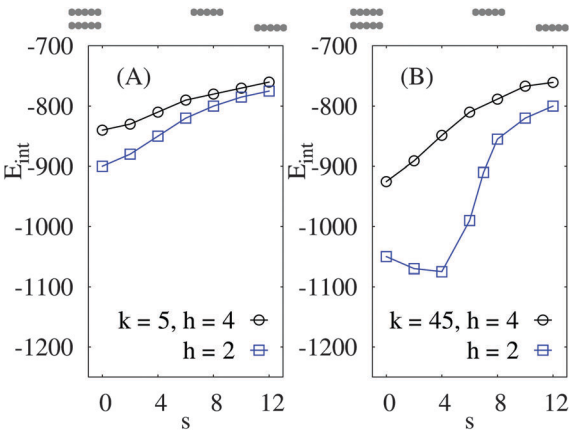

Fig. 10 Interaction energy of two rods sliding along each other at fixed inter-axial offset h and varying distance s, as indicated on the top of each panel. Parameters: $\varepsilon_A = 15$, $n = 25$. The energy values for large s and small h approach those for $d = s$ inter-rod separations shown in Fig. 8.

inter-axial distance h and varying horizontal shift s, see Fig. 1 for the notations. The centre-to-centre distance is then given by $d^2 = s^2 + h^2$. We observe that for soft sheets the interaction energy has a deep minimum for the two rods facing one another by their sides, for all offset values h between the rods, Fig. 10A. In this configuration with $s = 0$ the rods minimise the energy of network deformations around them. The radius of propagation of elastic deformations for these parameters is of the order of the distance h.

In contrast, for relatively stiff elastic sheets the interaction energy has a non-monotonic behaviour as a function of s for closely positioned particles, see the results at $h = 2a$ in Fig. 10B. At this conformation—due to long-ranged network deformations—the rods have little elastic substrate to share when they are positioned right on top on one another. Thus, E_{int} becomes less profitable at $s = 0$. At larger inter-axial distances h—apart from the overall decrease of E_{int} magnitude—the typical behaviour is similar to that for softer sheets, with a monotonically varying $E_{int}(s)$, see Fig. 10B for $h = 4a$.

IV. Discussion and conclusions

We analysed the substrate-mediated interactions of rod-like particles adsorbed on elastically responsive planar networks. We characterised the dependence of the rod–rod interaction energy on the mutual orientation angle β of the rods and the separation d between their centres. We showed that for soft elastic sheets the rods favour a tip-to-tip orientation, while for stiffer sheets rather a side-by-side arrangement is preferred energetically. For the force–distance curves of substrate-mediated rod–rod interactions we obtained that stronger rod–sheet attraction give rise to overall stronger interactions. We observed short-ranged repulsion and long-ranged attraction of rod-like particles, particularly pronounced for strong rod–sheet attraction. As the orientation angle β decreases from $\beta = \pi/2$ to $\beta = 0$, the minimum of the interaction energy shifts to larger distances d between the centres of the rods. By constructing the phase diagramme, we demonstrated to what extent the magnitude of inter-particle sheet-mediated interactions changes with the sheet elasticity and separation d. We also examined the attraction–repulsion behaviour when two adsorbed rods pass one another in a sliding fashion. We showed that for stiff sheets and close rod–rod inter-axial separations the interaction energy can be a non-monotonic function of the sliding distance s. For soft sheets the interaction energy varies monotonically with s, with the side-by-side configuration of rods.

In our work we characterise inter-rod tip-to-tip *versus* side-by-side substrate-mediated interactions as a function of the interface elastic properties, the inter-rod distance, and the strength of the particle–surface adhesion. Our findings thus provide new insights into collective deformations of elastic substrates as a response to the binding of elongated particles. We expect that *via* sensing curvature gradients of the substrate the rods can direct their assembly at a preferred orientation, when the particles are allowed to diffuse on supporting elastic sheets.[92]

Our simplistic two-dimensional system mimics the behaviour of negatively charged rod-like *fd* viruses on attractive cationic freestanding lipid membranes, as observed in experiments.[38] Adhesion of rod-like viruses onto cationic lipid membranes is driven by strong mutual electrostatic attraction and thereby involves local membrane deformations.[18] Based on the results of our simulations, the tip-to-tip assembly of *fd* viruses observed experimentally[38] should correspond to elastically soft membranes, which are easily deformable upon virus adhesion. For stiffer membranes we expect, on the contrary, the side-by-side arrangement of rods to be favourable.[127]

Open Access Article. Published on 28 July 2016. Downloaded on 1/24/2026 1:41:57 AM.
This article is licensed under a Creative Commons Attribution 3.0 Unported Licence.

This journal is © The Royal Society of Chemistry 2016

Open Access Article. Published on 28 July 2016. Downloaded on 1/24/2026 1:41:57 AM.
This article is licensed under a Creative Commons Attribution 3.0 Unported Licence.

Structural features of often highly charged and chiral filamentous viruses give rise to peculiar virus–virus interactions in solutions and along interfaces. In aqueous and polymer solutions, a multitude of ordered phases of filamentous viruses—including liquid crystalline, cholesteric, and smectic phases—are known to be formed.[106,107,113–115] It is of interest how the driving forces of assembly will be affected for a system of rod-like viruses when they are densely deposited on a free-standing lipid membrane. This process can, in principle, be tuned by membrane stiffness—particularly when cationic lipids partially envelope the negatively charged *fd* viruses—similarly as it is observed for polymer-coated sterically-stabilized virus particles.[107,113]

Our results can also provide some advantages for surface-based detection methods of relatively large viral and, particularly, bacterial pathogens, as compared to bulk-based detection techniques. For the latter, an impeded particle penetration into the responsive network often prohibits efficient particle detection, see the discussion in ref. 6 and 116. As a perspective for the future research—most importantly—a more realistic elastic sheet model of lipid membranes should be developed, to account for membrane–particle wrapping due to out-of-plane deformations. Also, asymmetric interface deformations induced by binding of *e.g.* Janus particles[117–120] with strongly heterogeneous adhesion properties may be considered. In particular, membrane-mediated aggregation of anisotropically curved banana-like Janus nanoparticles on large lipid vesicles was recently studied by simulations.[67] A wide range of particle–membrane adhesion, intrinsic particle curvature and particle density on the membrane was studied.[67] The membrane curvature due to anisotropic particle–membrane binding yields two main types of self-assembled structured: chain-like aggregates at weak bindings and asters at high adhesion strengths.[67] In the former, the nanoparticles prefer to stay parallel. In contrast, for strong particle–vesicle attraction strengths some three-armed stars are formed, due to saddle-like membrane deformations around them. At higher concentrations of adsorbed particles each aster is composed of three to six particles, see ref. 67.

Finally, the intriguing features of rod binding to attractive elastic sheets studied here can be applicable to translocation of chain-like polymeric molecules[121,122] across lipid membranes. In this setup, the molecule can partially adhere to the membrane surface on both sides, thereby affecting the kinetics and the scaling exponent of the translocation events.

References

1 E. Wischerhoff, N. Badi, J. F. Lutz and A. Laschewsky, Smart bioactive Surfaces, *Soft Matter*, 2010, **6**, 705.
2 F. Patolsky, G. Zheng, O. Hayden, M. Lakadamyali, X. Zhuang and C. M. Lieber, Electrical Detection of single Viruses, *Proc. Natl. Acad. Sci. U. S. A.*, 2004, **101**, 14017.
3 M. A. Cohen-Stuart, W. T. S. Huck, J. Genzer, M. Müller, C. Ober, M. Stamm, G. B. Sukhorukov, I. Szleifer, V. V. Tsukruk, M. Urban, F. Winnik, S. Zauscher, I. Luzinov and S. Minko, Emerging Applications of Stimuli-Responsive Polymer Materials, *Nat. Mater.*, 2010, **9**, 101.
4 R. Wang and Y. Li, Hydrogel Based QCM Aptasensor for Detection of *Avian Infuenza* Virus, *Biosens. Bioelectron.*, 2013, **42**, 148.
5 J. Liu, H. Liu, H. Kang, M. Donovan, Z. Zhu and W. Tan, Aptamer-Incorporated Hydrogels for visual Detection, controlled Drug Release, and targeted Cancer Therapy, *Anal. Bioanal. Chem.*, 2012, **402**, 187.
6 J. Shin, A. G. Cherstvy and R. Metzler, Sensing Viruses by mechanical Tension of DNA in responsive Hydrogels, *Phys. Rev. X*, 2014, **4**, 021002, and references cited therein.
7 H.-J. Wu, *et al.*, Membrane-Protein Binding measured with Solution-Phase plasmonic Nanocube Sensors, *Nat. Methods*, 2012, **9**, 1189.
8 I. Koltover, J. O. Rädler and C. R. Safinya, Membrane mediated Attraction and ordered Aggregation of colloidal Particles bound to giant phospholipid Vesicles, *Phys. Rev. Lett.*, 1999, **82**, 1991.
9 M. Simunovic, A. Srivastava and G. A. Voth, Linear Aggregation of Proteins on the Membrane as a Prelude to Membrane Remodeling, *Proc. Natl. Acad. Sci. U. S. A.*, 2013, **110**, 20396.
10 M. Simunovic and G. A. Voth, Membrane Tension controls the Assembly of Curvature-generating Proteins, *Nat. Commun.*, 2015, **6**, 7219.
11 M. Javanainen, H. Hammaren, L. Monticelli, J.-H. Jeon, M. S. Miettinen, H. Martinez-Seara, R. Metzler and I. Vattulainen, Anomalous and normal Diffusion of Proteins and Lipids in crowded Lipid Membranes, *Faraday Discuss.*, 2013, **161**, 397.
12 C. Eich, C. Manzo, S. de Keijzer, G.-J. Bakker, I. Reinieren-Beeren, M. F. Garcia-Parajo and A. Cambi, Changes in Membrane Sphingolipid Composition modulate Dynamics and Adhesion of Integrin Nanoclusters, *Sci. Rep.*, 2016, **6**, 20693.
13 H. Tang, H. Ye, H. W. Zhang and Y. Zheng, Wrapping of Nanoparticles by the Cell Membrane: the Role of Interactions between the Nanoparticles, *Soft Matter*, 2015, **11**, 8674.
14 C. Yolcu, R. C. Haussman and M. Deserno, The effective Field Theory Approach towards Membrane-mediated Interactions between Particles, *Adv. Colloid Interface Sci.*, 2014, **208**, 89.
15 B. J. Reynwar, G. Illya, V. A. Harmandaris, M. M. Müller, K. Kremer and M. Deserno, Aggregation and Vesiculation of Membrane Proteins by Curvature-mediated Interactions, *Nature*, 2007, **447**, 461.
16 C. Herold, P. Schwille and E. P. Petrov, DNA Condensation at freestanding cationic Lipid Bilayers, *Phys. Rev. Lett.*, 2010, **104**, 148102.
17 C. Herold, P. Schwille and E. P. Petrov, Single DNA Molecules on freestanding and supported cationic Lipid Bilayers: diverse conformational Dynamics controlled by the local Bilayer Properties, *J. Phys. D: Appl. Phys.*, 2016, **49**, 074001.
18 A. G. Cherstvy and E. P. Petrov, Modeling DNA Condensation on freestanding cationic Lipid Membranes, *Phys. Chem. Chem. Phys.*, 2014, **16**, 2020.

Open Access Article. Published on 28 July 2016. Downloaded on 1/24/2026 1:41:57 AM.
This article is licensed under a Creative Commons Attribution 3.0 Unported Licence.

19 G. B. Davies, T. Krueger, P. V. Coveney, J. Harting and F. Bresme, Assembling ellipsoidal Particles at fluid Interfaces using switchable dipolar capillary Interactions, *Adv. Mater.*, 2014, **26**, 6715.
20 A. Saric and A. Cacciuto, Self-Assembly of Nanoparticles adsorbed on fluid and elastic Membranes, *Soft Matter*, 2013, **9**, 6677.
21 A. Saric and A. Cacciuto, Mechanism of Membrane Tube Formation induced by adhesive Nanocomponents, *Phys. Rev. Lett.*, 2012, **109**, 188101.
22 J. C. Loudet, A. M. Alsayed, J. Zhang and A. G. Yodh, Capillary Interactions between anisotropic colloidal Particles, *Phys. Rev. Lett.*, 2005, **94**, 018301.
23 J. C. Loudet and B. Pouligny, Self-Assembled capillary Arrows, *Europhys. Lett.*, 2009, **85**, 28003.
24 P. S. Niemela, M. Miettinen, L. Monticelli, H. Hammaren, P. Bjelkmar, T. Murtola, E. Lindahl and I. Vattulainen, Membrane Proteins diffuse as dynamic Complexes with Lipids, *J. Am. Chem. Soc.*, 2010, **132**, 7574.
25 J.-H. Jeon, H. M. Monne, M. Javanainen and R. Metzler, Anomalous Diffusion of Phospholipids and Cholesterols in a Lipid Bilayer and its Origins, *Phys. Rev. Lett.*, 2012, **109**, 188103.
26 R. Metzler, J.-H. Jeon and A. G. Cherstvy, Non-Brownian Diffusion in lipid Membranes: Experiments and Simulations, *Biochim. Biophys. Acta, Biomembr.*, DOI: 10.1016/j.bbamem.2016.01.022.
27 J.-H. Jeon, M. Javanainen, H. Martinez-Seara, R. Metzler and I. Vattulainen, Protein Crowding in Lipid Bilayers gives rise to non-Gaussian anomalous lateral Diffusion of Phospholipids and Proteins, *Phys. Rev. X*, 2016, **6**, 021006.
28 G. R. Kneller, K. Baczynski and M. Pasenkiewicz-Gierula, Communication: Consistent Picture of lateral Subdiffusion in Lipid Bilayers: Molecular Dynamics Simulation and exact Results, *J. Chem. Phys.*, 2011, **135**, 141105.
29 S. Stachura and G. R. Kneller, Anomalous lateral Diffusion in Lipid Bilayers observed by Molecular Dynamics Simulations with atomistic and coarse-grained Force Fields, *Mol. Simul.*, 2014, **40**, 245.
30 C. Eggeling, *et al.*, Direct Observation of the Nanoscale Dynamics of Membrane Lipids in a living Cell, *Nature*, 2009, **457**, 1159.
31 V. Müller, C. Ringemann, A. Honigmann, G. Schwartzmann, R. Medda, M. Leutenegger, S. Polyakova, V. N. Belov, S. W. Hell and C. Eggeling, STED Nanoscopy reveals molecular Details of Cholesterol- and Cytoskeleton-Modulated Lipid Interactions in living Cells, *Biophys. J.*, 2011, **101**, 1651.
32 L. Botto, E. P. Lewandowski, M. Cavallaro Jr. and K. J. Stebe, Capillary Interactions between Anisotropic Particles, *Soft Matter*, 2012, **8**, 9957.
33 M. Cavallaro Jr., L. Botto, E. P. Lewandowski, M. Wang and K. J. Stebe, Curvature-Driven Capillary Migration and Assembly of Rod-like Particles, *Proc. Natl. Acad. Sci. U. S. A.*, 2011, **108**, 20923.
34 E. P. Lewandowski, J. A. Bernate, A. Tseng, P. C. Searson and K. J. Stebe, Oriented Assembly of anisotropic Particles by capillary Interactions, *Soft Matter*, 2009, **9**, 886.
35 J. O. Rädler, I. Koltover, T. Salditt and C. R. Safinya, Structure of DNA-Cationic Liposome Complexes: DNA Intercalation in multilamellar Membranes in distinct interhelical Packing Regimes, *Science*, 1997, **275**, 810.
36 I. Koltover, T. Salditt, J. O. Rädler and C. R. Safinya, An inverted hexagonal Phase of cationic Liposome–DNA Complexes related to DNA Release and Delivery, *Science*, 1998, **281**, 78.
37 A. G. Cherstvy, Electrostatics of DNA Complexes with Cationic Lipid Membranes, *J. Phys. Chem. B*, 2007, **111**, 7914.
38 A. B. Artemieva, C. Herold and E. P. Petrov, Interaction of semi-Flexible Filamentous Virus Particles with freestanding lipid Membranes, 2016, work in preparation.
39 B. Maier and J. O. Rädler, Conformation and Self-Diffusion of single DNA Molecules confined to Two Dimensions, *Phys. Rev. Lett.*, 1999, **82**, 1911.
40 I. Koltover, K. Wagner and C. R. Safinya, DNA Condensation in Two Dimensions, *Proc. Natl. Acad. Sci. U. S. A.*, 2000, **97**, 14046.
41 G. Witz, K. Rechendorff, J. Adamcik and G. Dietler, Conformation of Ring Polymers in 2D constrained Environments, *Phys. Rev. Lett.*, 2011, **106**, 248301.
42 F. Valle, M. Favre, P. De Los Rios, A. Rosa and G. Dietler, Scaling Exponents and Probability Distributions of DNA End-to-End Distance, *Phys. Rev. Lett.*, 2005, **95**, 158105.
43 J.-H. Jeon, J. Adamcik, G. Dietler and R. Metzler, Supercoiling Induces Denaturation Bubbles in circular DNA, *Phys. Rev. Lett.*, 2010, **105**, 208101.
44 E. Ercolini, F. Valle, J. Adamcik, G. Witz, R. Metzler, P. De Los Rios, J. Roca and G. Dietler, Fractal Dimension and Localization of DNA Knots, *Phys. Rev. Lett.*, 2007, **98**, 058102.
45 J. Adamcik, J.-H. Jeon, K. J. Karczewski, R. Metzler and G. Dietler, Quantifying Supercoiling-induced Denaturation Bubbles in DNA, *Soft Matter*, 2012, **8**, 8651.
46 A. Zinchenko, DNA conformational Behavior and Compaction in biomimetic Systems: Toward better Understanding of DNA Packaging in Cell, *Adv. Colloid Interface Sci.*, 2016, **232**, 70.
47 G. Luque-Caballero, J. Maldonado-Valderrama, M. Quesada-Perez and A. Martin-Molina, Atomic Force Microscopy as a Tool to study the Adsorption of DNA onto Lipid Interfaces, *Microsc. Res. Tech.*, 2016, DOI: 10.1002/jemt.22654.
48 D. Harries, S. May, W. M. Gelbart and A. Ben-Shaul, Structure, Stability, and Thermodynamics of lamellar DNA–Lipid Complexes, *Biophys. J.*, 1998, **75**, 159.
49 S. May, D. Harries and A. Ben-Shaul, The Phase Behavior of cationic Lipid–DNA Complexes, *Biophys. J.*, 2000, **78**, 1681.
50 H. Schiessel and H. Aranda-Espinoza, Electrostatically induced Undulations of lamellar DNA–Lipid Complexes, *Eur. Phys. J. E: Soft Matter Biol. Phys.*, 2001, **5**, 499.
51 C. Fleck, R. R. Netz and H. H. von Grünberg, Poisson–Boltzmann Theory for Membranes with mobile charged Lipids and the pH-dependent Interaction of a DNA Molecule with a Membrane, *Biophys. J.*, 2002, **82**, 76.
52 T. R. Weikl, Indirect Interactions of Membrane-Adsorbed Cylinders, *Eur. Phys. J. E: Soft Matter Biol. Phys.*, 2003, **12**, 265.

 This journal is © The Royal Society of Chemistry 2016

Open Access Article. Published on 28 July 2016. Downloaded on 1/24/2026 1:41:57 AM.
This article is licensed under a Creative Commons Attribution 3.0 Unported Licence.

53 M. Deserno, When do fluid Membranes engulf sticky Colloids?, *J. Phys.: Condens. Matter*, 2004, **16**, S2061.
54 M. Deserno and T. Bickel, Wrapping of a Spherical Colloid by a Fluid Membrane, *Europhys. Lett.*, 2003, **62**, 767.
55 M. Deserno, Elastic Deformation of a Fluid Membrane upon Colloid Binding, *Phys. Rev. E: Stat., Nonlinear, Soft Matter Phys.*, 2004, **69**, 031903.
56 C. C. Fleck and R. R. Netz, Electrostatic Colloid–Membrane Binding, *Europhys. Lett.*, 2004, **67**, 314.
57 A. H. Bahrami, R. Lipowski and T. R. Weikl, Tubulation and Aggregation of Spherical Nanoparticles Adsorbed on Vesicle, *Phys. Rev. Lett.*, 2012, **109**, 188102.
58 A. H. Bahrami, Orientational Changes and impaired Internalization of ellipsoidal Nanoparticles by Vesicle Membranes, *Soft Matter*, 2013, **9**, 8642.
59 D. S. Dean, T. C. Hammant, R. R. Horgan, A. Naji and R. Podgornik, Wrapping Transition and Wrapping-mediated Interactions for discrete Binding along an elastic Filament: An Exact Solution, *J. Chem. Phys.*, 2012, **137**, 144904.
60 D. Harries, S. May and A. Ben-Shaul, Counterion Release in Membrane–Biopolymer Interactions, *Soft Matter*, 2013, **9**, 9268.
61 X. Yi and H. Gao, Cell-Membrane Wrapping of a spherical thin elastic Shell, *Soft Matter*, 2015, **11**, 1107.
62 M. Raatz, R. Lipowsky and T. R. Weikl, Cooperative Wrapping of Nanoparticles by Membrane Tubes, *Soft Matter*, 2014, **10**, 3570.
63 L. Chen, S. Xiao, H. Zhu, L. Wang and H. Liang, Shape-dependent Internalization Kinetics of Nanoparticles by Membranes, *Soft Matter*, 2016, **12**, 2632.
64 A. H. Bahrami, R. Lipowsky and T. R. Weikl, The Role of Membrane Curvature for the Wrapping of Nanoparticles, *Soft Matter*, 2016, **12**, 581.
65 E. P. Lewandowski, M. Cavallaro Jr., I. Botto, J. C. Bernate, V. Garbin and K. J. Stebe, Orientation and Self-Assembly of cylindrical Particles by anisotropic capillary Interactions, *Langmuir*, 2010, **26**, 15142.
66 S. Ghosh, A. G. Cherstvy and R. Metzler, Deformation Propagation in responsive Polymer Network Films, *J. Chem. Phys.*, 2014, **141**, 074903.
67 A. D. Olinger, E. J. Spangler, P. B. S. Kumar and M. Laradji, Membrane-mediated Aggregation of anisotropically curved Nanoparticles, *Faraday Discuss.*, 2016, **186**, 265.
68 T. Noda, H. Ebihara, Y. Muramoto, K. Fujii, A. Takada, H. Sagara, J. H. Kim, H. Kida, H. Feldmann and Y. Kawaoka, Assembly and Budding of Ebolavirus, *PLoS Pathog.*, 2006, **2**, e99.
69 S. Welsch, L. Kolesnikova, V. Krähling, J. D. Riches, S. Becker and J. A. G. Briggs, Electron Tomography reveals the Steps in Filovirus Budding, *PLoS Pathog.*, 2010, **6**, e1000875.
70 R. R. Netz and D. Andelman, Neutral and charged Polymers at Interfaces, *Phys. Rep.*, 2003, **380**, 1.
71 A. V. Dobrynin and M. Rubinstein, Theory of Polyelectrolytes in Solutions and at Surfaces, *Prog. Polym. Sci.*, 2005, **30**, 1049.
72 A. Y. Grosberg, T. T. Nguyen and B. I. Shklovskii, Colloquium: The Physics of Charge Inversion in chemical and biological Systems, *Rev. Mod. Phys.*, 2002, **74**, 329.
73 A. G. Cherstvy, Electrostatic Interactions in biological DNA-related Systems, *Phys. Chem. Chem. Phys.*, 2011, **13**, 9942.
74 S. L. Brenner and V. A. Parsegian, A Physical Method for Deriving the electrostatic Interaction between Rod-like Polyions at all mutual Angles, *Biophys. J.*, 1974, **14**, 327.
75 A. A. Kornyshev, D. J. Lee, S. Leikin and A. Wynveen, Structure and Interactions of biological Helices, *Rev. Mod. Phys.*, 2007, **79**, 943.
76 D. J. Lee, R. Cortini, A. P. Korte, E. L. Starostin, G. H. M. van der Heijden and A. A. Kornyshev, Chiral Effects in Dual-DNA Braiding, *Soft Matter*, 2013, **9**, 9833.
77 A. G. Cherstvy and R. Everaers, Layering, Bundling, and azimuthal Orientations in dense Phases of Nucleosome Core Particles, *J. Phys.: Condens. Matter*, 2006, **18**, 11429.
78 S. McLaughlin, The electrostatic Properties of Membranes, *Annu. Rev. Biophys. Biophys. Chem.*, 1989, **18**, 113.
79 G. Cevc, Membrane Electrostatics, *Biochim. Biophys. Acta*, 1990, **1031–3**, 311.
80 D. Andelman, Electrostatic Properties of Membranes: the Poisson–Boltzmann Theory, in *Handbook of Biological Physics*, ed. R. Lipowsky and E. Sackmann, Elsevier, 1995, ch. 12, pp. 603–641.
81 R. Lipowsky, Generic Interactions of flexible Membranes, in *Handbook of Biological Physics*, ed. R. Lipowsky and E. Sackmann, Elsevier, 1995, ch. 11, pp. 521–602.
82 E. J. A. Veldhuizen and H. P. Haagsman, Role of pulmonary Surfactant Components in Surface Film Formation and Dynamics, *Biochim. Biophys. Acta*, 2000, **1467**, 255.
83 J. Perez-Gil, Structure of pulmonary Surfactant Membranes and Films: The Role of Proteins and Lipid–Protein Interactions, *Biochim. Biophys. Acta*, 2008, **1778**, 1676.
84 Y. Y. Zuo, R. A. W. Veldhuizen, A. W. Neumann, N. O. Petersen and F. Possmayer, Current Perspectives in pulmonary Surfactant-Inhibition, Enhancement and Evaluation, *Biochim. Biophys. Acta*, 2008, **1778**, 1947.
85 D. Stamou, C. Duschl and D. Johannsmann, Long-Range Attraction between colloidal Spheres at the Air–Water Interface: The Consequence of an irregular Meniscus, *Phys. Rev. E: Stat., Nonlinear, Soft Matter Phys.*, 2000, **62**, 5263.
86 P. A. Kralchevsky, N. D. Denkov and K. Danov, Particles with an undulated Contact Line at a fluid Interface: Interaction between capillary Quadrupoles and Rheology of particulate Monolayers, *Langmuir*, 2001, **17**, 7694.
87 J. B. Fournier and P. Galatola, Anisotropic capillary Interactions and Jamming of Colloidal Particles trapped at a Liquid–Fluid Interface, *Phys. Rev. E: Stat., Nonlinear, Soft Matter Phys.*, 2002, **65**, 031601.
88 S. Dasgupta, T. Auth and G. Gompper, Wrapping of ellipsoidal Nanoparticles by fluid Membranes, *Soft Matter*, 2013, **9**, 5473.
89 S. Dasgupta, T. Auth and G. Gompper, Shape and Orientation Matter for the cellular Uptake of nonspherical Particles, *Nano Lett.*, 2014, **14**, 687.

Open Access Article. Published on 28 July 2016. Downloaded on 1/24/2026 1:41:57 AM.
This article is licensed under a Creative Commons Attribution 3.0 Unported Licence.

90 S. Dasgupta, M. Katava, M. Faraj, T. Auth and G. Gompper, Capillary Assembly of Microscale ellipsoidal, cuboidal, and spherical Particles at Interfaces, *Langmuir*, 2014, **30**, 11873.
91 Z. Shi and T. Baumgart, Dynamics and Instabilities of Lipid Bilayer Membrane Shapes, *Adv. Colloid Interface Sci.*, 2014, **208**, 76.
92 S. K. Ghosh *et al.*, work in progress, 2016.
93 E. A. Evans, R. Waugh and L. Melnik, Elastic Area Compressibility Modulus of red Cell Membrane, *Biophys. J.*, 1976, **16**, 585.
94 A. J. Kosmalska, *et al.*, Physical Principles of Membrane Remodelling during Cell Mechanoadaptation, *Nat. Commun.*, 2015, **6**, 7292.
95 A. G. Clark, O. Wartlick, G. Salbreux and E. K. Paluch, Stresses at the Cell Surface during Animal Cell Morphogenesis, *Curr. Biol.*, 2014, **24**, R484.
96 M. Staykova, M. Arroyo, M. Rahimi and H. A. Stone, Confined Bilayers passively regulate Shape and Stress, *Phys. Rev. Lett.*, 2013, **110**, 028101.
97 A. Diz-Munoz, D. A. Fletcher and O. D. Weiner, Use the Force: Membrane Tension as an Organizer of Cell Shape and Motility, *Trends Cell Biol.*, 2013, **23**, 47.
98 J. R. Hendriksen and J. H. Ipsen, Measurement of Membrane Elasticity by Micro-Pipette Aspiration, *Eur. Phys. J. E: Soft Matter Biol. Phys.*, 2004, **14**, 149.
99 Y. Chen, B. Lu, Y. Chen and X. Feng, Breathable and stretchable Temperature Sensors inspired by Skin, *Sci. Rep.*, 2015, **5**, 11505.
100 J. A. Rogers, *et al.*, Materials and Mechanics for stretchable Electronics, *Science*, 2010, **327**, 1603.
101 C. Mohrdieck, A. Wanner, W. Roos, A. Roth, E. Sackmann, J. P. Spatz and E. Arzt, A Theoretical Description of elastic Pillar Substrates in biophysical Experiments, *ChemPhysChem*, 2005, **6**, 1492.
102 W. H. Roos, A. Roth, J. Konle, H. Presting, E. Sackmann and J. P. Spatz, Freely suspended Actin Cortex Models on Arrays of microfabricated Pillars, *ChemPhysChem*, 2003, **4**, 872.
103 C. Monzel, S. F. Fenz, M. Giesen, R. Merkel and K. Sengupta, Mapping Fluctuations in Biomembranes adhered to Micropatterns, *Soft Matter*, 2012, **8**, 6128.
104 M. Kocun, T. D. Lazzara, C. Steinem and A. Janshoff, Preparation of Solvent-Free, Pore-Spanning Lipid Bilayers: Modeling the Low Tension of Plasma Membranes, *Langmuir*, 2011, **27**, 7672.
105 N. Dharan and O. Farago, Formation of Adhesion Domains in stressed and confined Membranes, *Soft Matter*, 2015, **11**, 3780.
106 E. Barry, D. Beller and Z. Dogic, A Model Liquid crystalline System based on rodlike Viruses with variable Chirality and Persistence Length, *Soft Matter*, 2009, **5**, 2563.
107 Z. Dogic and S. Fraden, Ordered Phases of filamentous Viruses, *Curr. Opin. Colloid Interface Sci.*, 2006, **11**, 47.
108 L. A. Day, C. J. Marzec, S. A. Reisberg and A. Casadevall, DNA Packaging in filamentous Bacteriophages, *Annu. Rev. Biophys. Biophys. Chem.*, 1988, **17**, 509.
109 E. Loh, Quasielastic Light Scattering from Solutions of filamentous Viruses. II. Comparison between Theories and Experiments, *Biopolymers*, 1979, **18**, 2569.
110 T. Maeda and S. Fujime, Dynamic Light-scattering Study of Suspensions of fd-Virus. Application of a Theory of the Light-scattering Spectrum of weakly bending Filaments, *Macromolecules*, 1985, **18**, 2430.
111 J. D. Weeks, D. Chandler and H. C. Andersen, Role of repulsive Forces in determining the Equilibrium Structure of simple Liquids, *J. Chem. Phys.*, 1971, **54**, 5237.
112 M. P. Allen and D. J. Tildesley, *Computer Simulations of Liquids*, Clarendon Press, Oxford UK, 1987.
113 Z. Dogic and S. Fraden, Development of model colloidal Liquid Crystals and the Kinetics of the isotropic-smectic Transition, *Philos. Trans. R. Soc. London, Ser. A*, 2001, **359**, 997.
114 Z. Dogic and S. Fraden, Cholesteric Phase in Virus Suspensions, *Langmuir*, 2000, **16**, 7820.
115 Z. Dogic and S. Fraden, Smectic Phase in a colloidal Suspension of semiflexible Virus Particles, *Phys. Rev. Lett.*, 1997, **78**, 2417.
116 A. Godec, M. Bauer and R. Metzler, Collective Dynamics effect transient Subdiffusion of inert Tracers in flexible Gel Networks, *New J. Phys.*, 2014, **16**, 092002.
117 A. Walther and A. H. E. Müller, Janus Particles, *Soft Matter*, 2008, **4**, 663.
118 Q. Xie, G. B. Davies, F. Günther and J. Harting, Tunable dipolar capillary Deformations for magnetic Janus Particles at Fluid–Fluid Interfaces, *Soft Matter*, 2015, **11**, 3581.
119 T. Brugarolas, B. J. Park, M. H. Lee and D. Lee, Generation of amphiphilic Janus Bubbles and their Behavior at an Air–Water Interface, *Adv. Funct. Mater.*, 2011, **21**, 3924.
120 S. J. de Calvalho, R. Metzler and A. G. Cherstvy, Critical Adsorption of Polyelectrolytes onto charged Janus Nanospheres, *Phys. Chem. Chem. Phys.*, 2014, **16**, 15539.
121 M. Muthukumar, *Polymer Translocation*, CRC Press, Boca Raton, Florida, 2011.
122 V. V. Palyulin, T. Ala-Nissila and R. Metzler, Polymer Translocation: the first two Decades and the recent Diversification, *Soft Matter*, 2014, **10**, 9016.
123 Also, the effect of varying length-to-thickness ratio of rodlike protein particles was examined. Here, more elongated shapes were shown to give rise to side-by-side assembly at increasing membrane tension Σ, while shorter particles aggregate in a tip-to-tip manner.[10] Higher tensions suppress membrane fluctuations thus inhibiting the formation of long-living linear aggregates with tip-to-tip contacts.[10] An increase of tension from zero to 1.8 mN m^{-1} was *e.g.* shown to reduce the polymerisation energy of BAR proteins on the membrane from 12 to only 3 k_BT and substantially reduce the protein–protein interaction range from about 125 to 50 Å.[10] The reduction of the interaction range with Σ agrees with the theoretical length scale of membrane deformations, $\Lambda = \sqrt{\kappa/\Sigma} \sim \Sigma^{-1/2}$. Lipid bilayers with higher bending rigidities were shown to guide the proteins toward the side-by-side configuration.[10]

Open Access Article. Published on 28 July 2016. Downloaded on 1/24/2026 1:41:57 AM.
This article is licensed under a Creative Commons Attribution 3.0 Unported Licence.

124 Other approximations used are as follows. (a) We consider only deformation-mediated interactions of rods. For experimentally related low-salt buffers the presence of electrostatic orientation-dependent forces[74] could also contribute to the orientation trends of interacting rods, as described here. (b) The rods are of a finite length, while the elastic lattice is relatively large to minimise boundary effects. In the future, the implications of more formal and exact periodic boundary conditions will be investigated.[92] (c) We use the primitive model to mimic the effects of binding of elongated colloidal particles to lipid membranes.

125 One way is to relate the rod–rod interaction energies to the overall binding energy of N_b network beads bound to the ith rod $i = 1, 2$ that is $E_A = -\varepsilon_A N_{i,b}$. This energy triggers network deformations and (after subtracting the rods' self-energies on the network) defines the magnitude of E_{int}. So, the relation $|\varepsilon_A N_{1,b} + \varepsilon_A N_{2,b}| > (E_{1,el} + E_{2,el}) > E_{int}$ is valid. Another way is to measure the pair-wise rod–rod interaction energies in absolute values, namely in units of $k_B T$. This energy finally governs the preferences for the mutual aggregation of diffusing *fd* viruses on freestanding cationic lipid membranes in experiments.[38]

126 Note that for $\beta = \pi/2$ the minimal centre-to-centre distance between the rods is smaller than in Fig. 8A and B, namely $d_{min} = 2a$. In this setup the configuration with $\beta = \pi/2$ and $d = 1a$ corresponds to the rods touching by their sides. Therefore, as β approaches $\pi/2$ the minimum of E_{int} shifts to shorter d, Fig. 8.

127 Note however that effectively non-zero membrane tensions on some membrane vesicles might shift the energetic preferences of tip-to-tip *versus* side-by-side configurations. This effect might be the point of future investigations, both *in vitro* and *in silico*, bearing in mind the importance of membrane tension for functioning and aggregation of membrane-bound proteins.[24]